



Cite this: *Soft Matter*, 2022, 18, 9026

Adjusting the water-sensitivity of sugar/boronate-based organogels†

Andreas D. Ludwig,^a Noémie Ourvois-Maloisel,^b Arnaud Saint-Jalmes,^b Franck Artzner,^b Jean-Paul Guégan,^a Olivier Tasseau,^a Fabienne Berrée*^a and Loïc Lemiègre *^a

During the investigation of the water-sensitivity of (arylboronate alkylglucoside)-based organogels, we evaluated a series of twelve potential organogelators. They were synthesised in a single step from the corresponding arylboronic acids and alkylglucosides. Eight of them showed organogelation abilities in three solvents (toluene, cyclohexane, and ethyl myristate). Conformational minimisations of the potential organogelators permitted a clear relationship between the arylboronate orientation and the gelation effectiveness to be established. These gels were characterised by rheometry and SEM which revealed a gel-state originating from the self-assembly of the organogelators into long entangled fibres. SAXS confirmed the mode of packing in a hexagonal phase. Gels in toluene were found to be water-sensitive both after addition of a small amount of water and immersion into water. This study demonstrated that the main parameter impacting the water-sensitivity was the length of the alkyl chain at the anomeric position of the glucoside unit, much more than the functionalisation of an arylboronate moiety.

Received 29th September 2022,
Accepted 2nd November 2022

DOI: 10.1039/d2sm01305c

rsc.li/soft-matter-journal

Introduction

Organogels refer to the immobilisation of an organic solvent in the presence of a suitable gelator. Polymeric networks usually provide chemical organogels whereas the hierarchical self-assembly of small molecules belongs to physical gels. Indeed, the latter results from the formation of a 3D network based on low energy interactions between organogelators.^{1–5} The ability of low molecular weight compounds to behave like organogelators is linked to their solubility/aggregation balance in a given solvent and therefore to their capacity to self-assemble through van der Waals, hydrogen bonding or/and π - π interactions.^{6,7} Several groups already rationalized the gelation ability of organogelators as a function of solvent parameters, permitting gelation in a given solvent to be predicted.^{7–10} Sugar-based organogelators have played an important role in the development of organogels. They offer an interesting platform which can be further equipped with interacting groups (alkyl chains, aromatic rings, esters, amides, ureas, *etc.*)^{11–13} Recently, research groups have taken advantage of the self-assembly process to develop responsive

organogels to various stimuli such as heat, light, sound, ions, and redox conditions.^{14–23}

Within this context, sugar-boronate derivatives constitute a recent family of organogelators which already produced gels in various solvents (Fig. 1).²⁴ Starting from the readily available glucoside, the selective reaction of boronic acids on positions 4,6 of the glucoside represents an easy access to these molecules. Their chemical structures are very similar to those of benzylidene ones,^{25–35} except for a boron atom instead of acetalic carbon. Compared to the benzylidene function, the boronate one affords a slightly different geometry and remarkable water sensitivity which deserve to be investigated in depth. These water-sensitive gels might find applications in drug delivery for topical medicines or as appropriate ingredients for care lotions or cosmetic formulations. Furthermore, similar gelators exhibit important luminescent properties.^{36,37} Using these boronate/sugar-based organogelators bearing water-sensitive properties could lead to water detection systems. Thus, with the aim to understand and to adjust the water-sensitivity of these organogels, we designed a novel series of sugar-boronate organogelators bearing structural variations both on the aromatic ring of phenylboronate and at the anomeric position of the glucoside (*i.e.* aglycone) (Fig. 1). Indeed, the length of the aglycone alkyl chain might impact the hydrophobicity of the gels and different substitutions on the aromatic ring of the boronate would modify the water-sensitive properties of this function. It is already known that increasing the steric hindrance around the boron atom (*o*-CH₃, *o*-CF₃) dramatically reduces the hydrolysis kinetics of such boronates.

^a Univ Rennes, Ecole Nationale Supérieure de Chimie de Rennes, CNRS, ISCR – UMR6226, F-35000 Rennes, France. E-mail: loic.lemiegre@ensc-rennes.fr

^b Univ Rennes, CNRS, IPR (Institut de Physique de Rennes) – UMR 6251, F-35000 Rennes, France

† Electronic supplementary information (ESI) available: NMR spectra, rheometry, SEM, SAXS, hydrolysis experiments, and computational details. See DOI: <https://doi.org/10.1039/d2sm01305c>

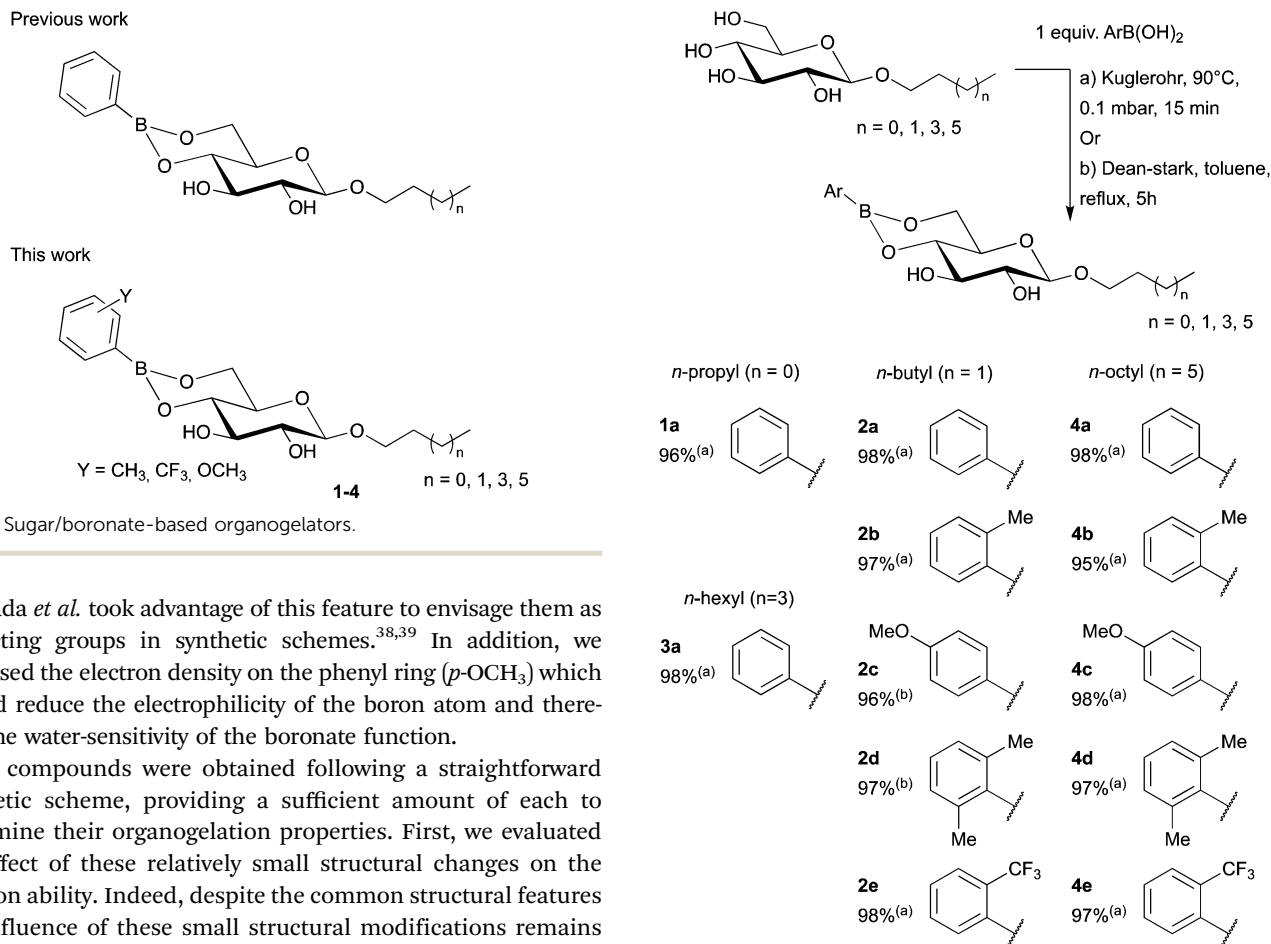


Fig. 1 Sugar/boronate-based organogelators.

Shimada *et al.* took advantage of this feature to envisage them as protecting groups in synthetic schemes.^{38,39} In addition, we increased the electron density on the phenyl ring (*p*-OCH₃) which should reduce the electrophilicity of the boron atom and therefore the water-sensitivity of the boronate function.

All compounds were obtained following a straightforward synthetic scheme, providing a sufficient amount of each to determine their organogelation properties. First, we evaluated the effect of these relatively small structural changes on the gelation ability. Indeed, despite the common structural features the influence of these small structural modifications remains difficult to predict and might enhance or prevent the gelation of a given solvent. The corresponding organogels were then characterised by rheometry, SEM and SAXS. Finally, their water-sensitivities were evaluated upon exposure to a small amount or a large excess of water. Thus, this study offers to decipher the main molecular parameters favouring the gelation and/or responsible for the water-sensitivity of such organogels.

Results and discussion

Synthesis

Arylboronate alkylglucosides **1-4** were prepared from the readily available alkyl glucosides in one single step. In fact, the formation of a boronate function requires only the presence of boronic acid, a diol, and the removal of two water molecules (Scheme 1). Applied to alkyl glucosides, the reaction is regioselective towards the formation of 4,6-boronate isomers only.⁴⁰ Two experimental procedures were used to perform this esterification, both involved the displacement of the equilibrium by removing water molecules produced during transformation. Simple heating (90 °C) in a Kugelrohr oven, at a reduced pressure (0.1 mbar) and without solvent, provided most of the time successful reactions and excellent yields (95 to 98%) after only 15 min. When these solvent free conditions were not efficient enough due to incorrect mixing of the two powders, for **2c** and **2d**, we used a Dean-Stark apparatus with toluene as a

Scheme 1 Synthesis of aromatic boronate alkylglucosides **1-4**.

solvent which led to complete reactions after few hours (5 h) with excellent yields (96–97%). As expected, the regioselectivity was fully in favour of the formation of the boronate function at the position 4,6 of the alkylglucoside as confirmed by NMR analysis. This series of 12 arylboronate alkylglucosides were then engaged in gelation assays.

Gelation assays

The gelation ability of each compound was evaluated in several solvents including three representative ones: an aromatic solvent (toluene), an alkane (cyclohexane) and a biocompatible solvent (ethyl myristate).⁴¹ The goal of this evaluation was to determine the impact of small structural modifications (Scheme 1) on the gelation of organic solvents. In general, all compounds were soluble in ethyl acetate, dichloromethane, chloroform, THF and dioxane and insoluble in diisopropylether. Concerning toluene, cyclohexane and ethyl myristate, the results are shown in Table 1. The four phenylboronate derivatives (**1a-4a**, *n*-propyl, *n*-butyl, *n*-hexyl, and *n*-octyl) gave gels in toluene at similar minimal gelation concentrations (MGCs) around 10–12 mg mL⁻¹. These MGCs were slightly dependent on the length of the alkyl chain, with a lowest MGC for the hexyl derivative (**3a**). The chain length also modified the optical properties of the gels which were

Table 1 Gelation assays^a

| Compound | Toluene | Cyclohexane | Ethyl myristate |
|------------------|-------------------|-------------------|-------------------|
| 1a | G ^T 12 | G ^P 2 | G ^T 12 |
| 2a ²⁴ | G ^T 11 | G ^T 3 | G ^T 10 |
| 3a ²⁴ | G ^O 10 | I | G ^O 10 |
| 4a ²⁴ | G ^O 12 | I | G ^O 8 |
| 2b | G ^O 15 | I | G ^P 15 |
| 4b | G ^O 15 | G ^T 10 | G ^T 15 |
| 2c | G ^T 12 | I | G ^O 12 |
| 4c | G ^T 10 | G ^P 20 | G ^T 10 |
| 2d | S | S | S |
| 4d | S | S | S |
| 2e | S | S | S |
| 4e | S | S | S |

^a I: insoluble; S: soluble; P: precipitate; G^P: partial gel; G^T: translucent gel; G^O: opaque gel. The values indicate minimum gelation concentrations (MGCs) in mg mL⁻¹.

transparent for propyl and butyl derivatives (1a and 2a) but opaque for longer chains (3a and 4a). This observation clearly indicates that different degrees of crystallinity appeared within these materials which can be related to solubility effects. We determined the gelation domain in the Hansen space for compounds 2a and 4a following the methodology described by Bouteiller *et al.* (see the ESI,† S7 for graphs).⁷ Although our study was performed with a limited number of solvents, it seems that longer alkyl chains shift the centre of the gelation sphere and reduce the gelation domain. Therefore, opaque gels for 3a and 4a could be linked to reduced solubility compared to shorter chains (1a and 2a). Also, during VT ¹H NMR experiments, gels prepared with 2a, 3a and 4a in toluene showed broaden signals at 25 °C which are the characteristic of gel states. These broaden signals were maintained until 60 °C, from which the signals became sharp enough to observe all scalar couplings. Interestingly, no significant differences were observed between these gels, demonstrating that the chain length has a limited impact on the gel/sol transition temperature. In cyclohexane, the butyl derivative 2a provided the best gelation conditions, and it furnished a transparent gel at a very low MGC (3 mg mL⁻¹). In ethyl myristate, the MGC ranged from 8 to 12 mg mL⁻¹ with the lowest concentration for the octyl counterpart (4a). Therefore, an interesting finding that emerges from the first part of this work is that the gelation ability of these compounds can be adjusted to the solvent through a fine modulation of the length of the aglycone alkyl chain. Then, we evaluated the influence of phenyl ring substitutions, with the final aim to control the water-sensitivity of such gels.^{38,39} However, additional substituents on the phenyl ring also induced a modification of the gelation ability of these molecules. Indeed, the addition of one methyl at the *ortho* position of phenyl boronate (2b and 4b) increased the MGC of the gelation of toluene to 15 mg mL⁻¹. Also, the gelation of cyclohexane at 10 mg mL⁻¹ (4b) was obtained while 4a led to insoluble materials. Conversely, 2b gave insoluble materials while 2a was able to gel cyclohexane at a very low MGC. In ethyl myristate, 2b provided a partial gel only and 4b gelled this solvent but with an increased MGC compared to 4a.

The addition of a methoxy group at the *para* position of phenylboronate (2c and 4c) had a very little influence on the

gelation properties. 2c and 4c produced very similar results compared to the simpler phenyl boronate (2a and 4a) in both toluene and ethyl myristate. However, in cyclohexane, 2c remained insoluble and 4c did not provide a complete gelation even at a high concentration (4c, 20 mg mL⁻¹). It contrasted much with the results obtained with 2a (3 mg mL⁻¹). To reduce even more the water-sensitivity, we envisaged the substitution of the phenyl ring with two *o*-methyl groups (2d and 4d) or with one trifluoromethyl group (2e and 4e).^{38,39} These two modifications dramatically reduced the self-assembling properties of such compounds leading to solutions, even at concentrations higher than 20 mg mL⁻¹. Therefore, it demonstrated again that slight modulations of the molecular structure induce different or even opposite gelation capacities within this series of compounds.

Computational studies and conformations

Intrigued by the impact of these relatively small structural variations on the gelation abilities, we investigated the conformation of this series of alkylglucoside arylboronates (Scheme 1) by density functional theory methods. From previous published works on organoborate derivatives, several combinations of functional and basis sets were compared to obtain an accurate model of the arylboronate molecular structure (see the ESI,† Table S6.1). Geometric optimizations were carried out at the selected level of theory ωB97XD/cc-pVTZ, as recently used for phenylboronate, to consider weak interactions involved particularly between the aromatic core and the six-membered ring of the boronate function.^{42,43} The selected optimized geometries of 2a–e are shown in Fig. 2. As expected, the alkyl glucoside moieties have the same conformation for all compounds, but the aromatic ring ends with different orientations. Indeed, the aromatic core adopts a periplanar conformation for 2a, 2b, 2c which are effectively organogelators. However, in the presence of one *o*-CF₃ (2d) or two *o*-Me (2e), these molecules, which did not provide gels, show increased torsion angles (55° and 52°, respectively) with mainly a steric effect (see the ESI,† Table S6.2). Therefore, the self-assembly leading to the formation of gels

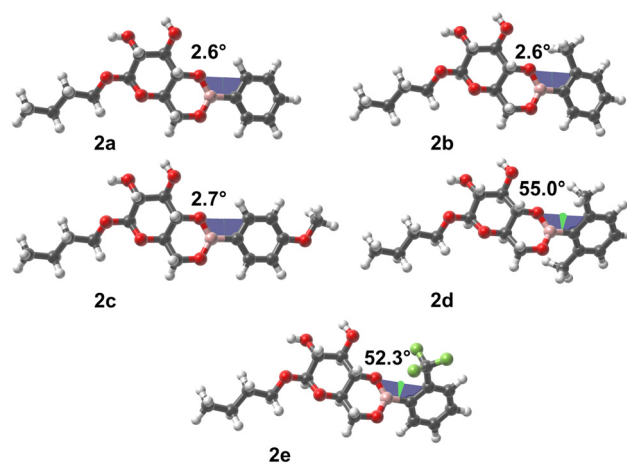


Fig. 2 DFT optimized conformations of *n*-butylglucoside arylboronates 2a–e.

seems to require a specific molecular geometry in which aryl-boronate must adopt a planar conformation. This conclusion is consistent with the mode of self-assembly that we demonstrated earlier for such compounds in which two aromatic rings are self-assembled through a herringbone packing.²⁴ Once the torsion angle increases, aromatic ring orientations modify the aromatic-aromatic interactions preventing an efficient self-assembly. Consequently, the gelation ability is dramatically reduced, explaining why **2d–e** and **4d–e** did not furnish gels.

Characterisation of the organogels

Rheometry. The mechanical properties of all gels were investigated by rheological amplitude-sweep experiments. Previously, we showed that the rheology of these gels was constant over a large range of frequency (see the ESI,† S2.1. for frequency dependent rheology experiments). Fig. 3 shows the graphs of G' and G'' against the applied strain obtained at a frequency of 1 Hz and at the MGC of each gelator in toluene (Graphs for other solvents are available in the ESI,† S2.2.). At low strain, all gels are characterized by storage moduli typically one order of magnitude higher than the loss moduli confirming the formation of gels that behave as elastic solids at small deformations (Table 2). However, the typical values of G' remain of the order of hundreds to a few

Table 2 Storage and loss moduli at low strain^a

| Compound | Solvent | G' | G'' | G'/G'' |
|-----------|--------------|------|-------|----------|
| 1a | Toluene | 1713 | 90 | 19.0 |
| 1a | Et myristate | 1149 | 78 | 14.7 |
| 2a | Toluene | 2724 | 213 | 12.8 |
| 2a | Cyclohexane | 326 | 40 | 8.1 |
| 2a | Et myristate | 1196 | 279 | 4.3 |
| 3a | Toluene | 1124 | 111 | 10.1 |
| 3a | Et myristate | 206 | 90 | 2.3 |
| 4a | Toluene | 753 | 341 | 2.2 |
| 4a | Et myristate | 1075 | 287 | 3.7 |
| 2b | Toluene | 1827 | 439 | 4.2 |
| 4b | Toluene | 1666 | 608 | 2.7 |
| 4b | Cyclohexane | 552 | 56 | 9.9 |
| 4b | Et myristate | 3508 | 298 | 11.8 |
| 2c | Toluene | 1521 | 160 | 9.5 |
| 2c | Et myristate | 763 | 229 | 3.3 |
| 4c | Toluene | 1955 | 205 | 9.5 |
| 4c | Et myristate | 1758 | 158 | 11.1 |

^a At strain <1%, 1 Hz frequency.

thousand of Pa, meaning rather soft gels. Among these organogelators, **1a** led to a gel with the most interesting rheological properties in toluene with a high G' value and the highest G'/G'' ratio. In ethyl myristate, **1a** also gave a high G'/G'' ratio while gelation from **4b** provided the highest G' value (3500 Pa). Note also that some gels present a clear plateau of G' at low strain, which is a signature of a linear elastic regime extending on a large range of amplitude (Fig. 3). Conversely, others (from **2a** and **4a–b**) have elastic properties always reducing as the deformation increases, meaning some intrinsic microscopic rearrangements even at low amplitudes of deformation. Consistently, it is for these gels that the ratio G'/G'' is the smallest. As this amplitude is further increased, all the gels show a yielding behaviour, with G'' eventually dominating. The deduced yield strains vary from 0.02 to 0.2 and depend strongly on the organogelators. Above these yield strains, which corresponds here to lower values for gels, the microstructure is irreversibly modified by the imposed shear. As shown in Fig. 3, the more the gel is initially elastic (high elastic moduli G' , and a well-defined plateau of G') the lower is its yield strain. Simultaneously, these measurements show that one can adjust the macroscopic gel texture and its yielding properties by tuning the molecular chemical structure of the organogelator.

Scanning electron microscopy

SEM images were recorded on xerogels obtained after removing the solvent of toluene-based gels (freeze-drying). Networks of fibres are easily observable in most of the samples (Fig. 4). Only **1a** and **2c** produced aggregated structures in which thin fibres are visible at high magnification (see the ESI,† S3). Except these two, fibres are in general few hundred μm long and less than 1 μm width. Keeping in mind that the drying process might cause collapse or other modifications of the fibrillar network, we are convinced that the fibres observed by SEM constitute a representative network responsible for the immobilisation of the solvent as gels. At least, it confirms that the gelation proceeded through the hierarchical self-assembly of the organogelator molecules.

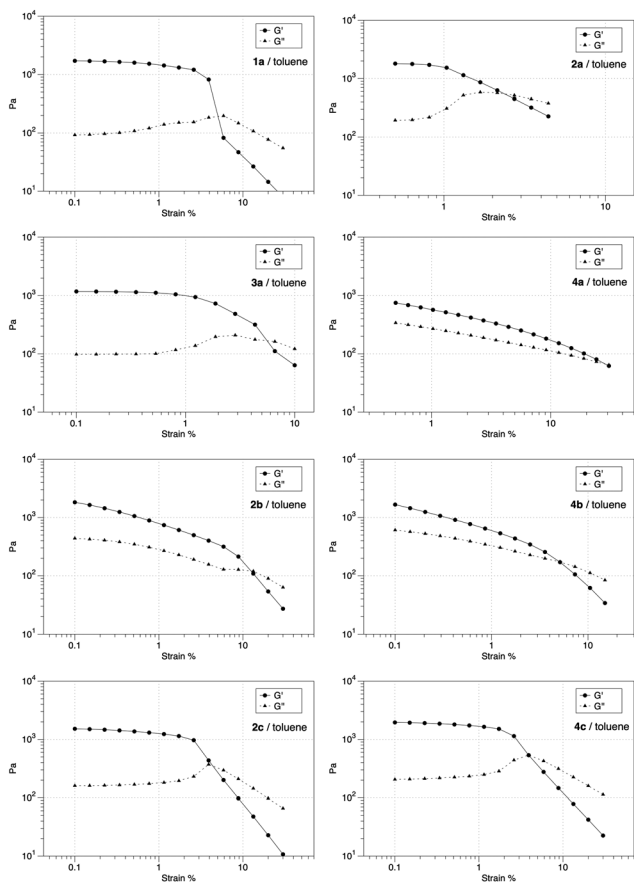


Fig. 3 Storage modulus (G' , plain line) and loss modulus (G'' , dashed line) against strain % of organogels obtained in toluene with organogelators **1–4**.

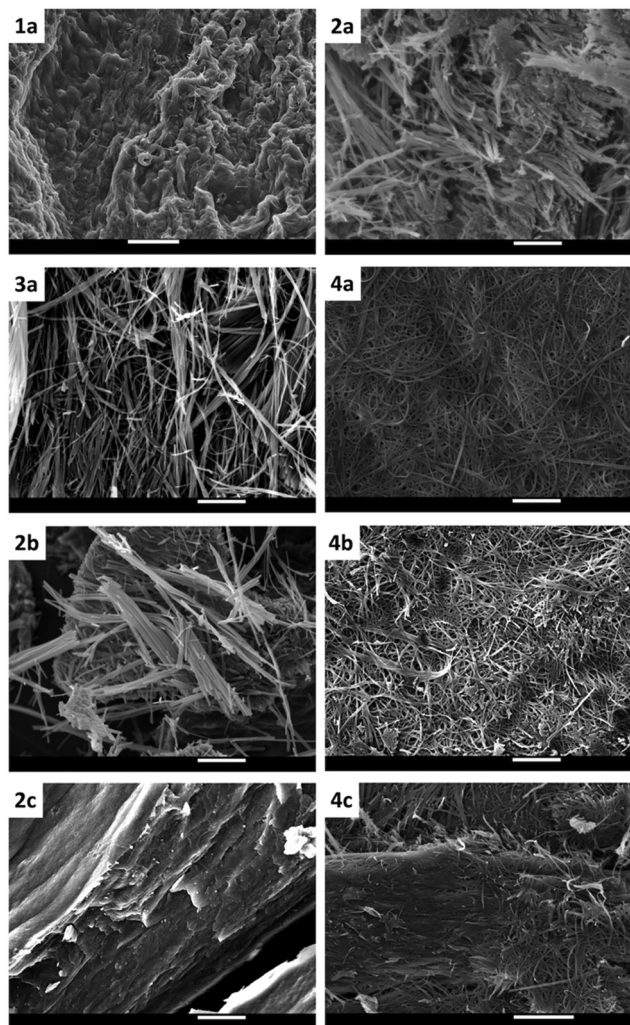


Fig. 4 SEM images of xerogels obtained from toluene-based gels. Scale bar: 10 μm .

Small-angle X-ray scattering

SAXS analysis can provide insights into the mode of packing involved in the self-assembly. We were lucky to obtain a well-resolved SAXS diagram for xerogels prepared using **4b** originally coming from gels in toluene and cyclohexane (Fig. 5, see the ESI†, S4 for cyclohexane). Both samples provided the superposable data from which we extracted the Bragg peaks gathered in Table 3. The corresponding indexation revealed the existence of a hexagonal phase which was assigned without any ambiguity. Consequently, tracing q_{hkl} in a hexagonal lattice, where h , k , and l refer to Miller indices, gave access to repeating parameters of $a = b = 27.4 \text{ \AA}$ and $c = 5.1 \text{ \AA}$. These lattice parameters are compatible with the organisation of the aromatic ring into herringbone packing and with the size of the organogelator (**4b**) (Fig. 6). It is noteworthy that this type of self-assembly was already described for **4a** with slightly different lattice parameters ($a = b = 26.8 \text{ \AA}$; $c = 5.5 \text{ \AA}$).²⁴ It is noteworthy that the similar lattice parameters observed for **4a** and **4b** support comparable conformations and torsion angles as estimated by

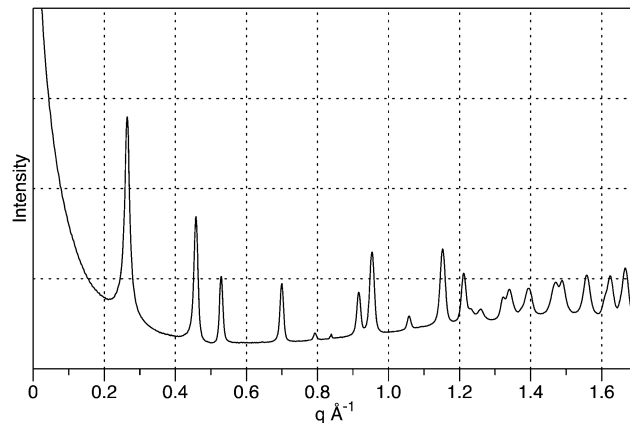


Fig. 5 SAXS profiles of xerogels obtained with **4b** (toluene).

Table 3 Theoretical and observed indexations of the hexagonal phase shown in Fig. 5 ($a = b = 27.4 \text{ \AA}$; $c = 5.1 \text{ \AA}$)

| h | k | l | Q_{calc}^a | Q_{obs}^b |
|-----|-----|-----|---------------------|--------------------|
| 1 | 0 | 0 | 0.2642 | 0.2642 |
| 1 | 1 | 0 | 0.4577 | 0.4578 |
| 2 | 0 | 0 | 0.5285 | 0.5286 |
| 2 | 1 | 0 | 0.6991 | 0.6991 |
| 3 | 0 | 0 | 0.7927 | 0.7929 |
| 2 | 2 | 0 | 0.9153 | 0.9153 |
| 3 | 1 | 0 | 0.9527 | 0.9526 |
| 4 | 0 | 0 | 1.0569 | 1.0570 |
| 3 | 2 | 0 | 1.1517 | 1.1513 |
| 4 | 1 | 0 | 1.2108 | 1.2103 |
| 1 | 0 | 1 | 1.2576 | 1.2580 |
| 1 | 1 | 1 | 1.3120 | 1.3195 |
| 2 | 0 | 1 | 1.3383 | 1.3383 |
| 4 | 2 | 0 | 1.3982 | 1.3894 |
| 3 | 0 | 1 | 1.4629 | 1.4636 |
| 3 | 1 | 1 | 1.5554 | 1.5560 |
| 4 | 0 | 1 | 1.6214 | 1.6218 |

^a Theoretical indexation. ^b Observed indexation.

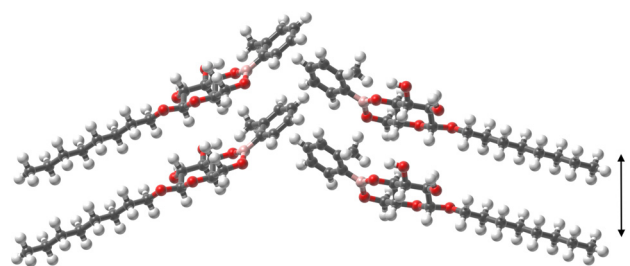
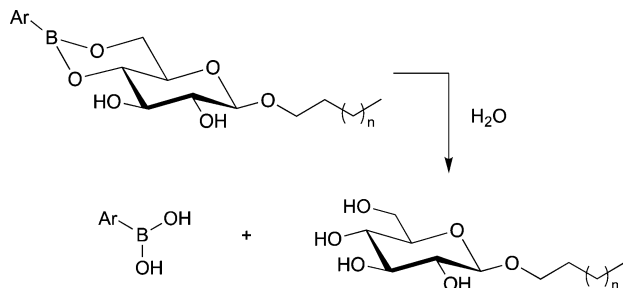


Fig. 6 Representation of the self-assembly of **4b** following a herringbone packing between aromatic rings. (The octyl chain are shown as extended for clarity).

the DFT method. Also, the crystal packing of the close boronate derivative (methyl-2-deoxy- α -D-glucopyranoside 4,6-phenylboronate) involves the same molecular arrangement.⁴⁴

Interested by the mode of packing of these compounds, we performed the SAXS analysis of all xerogels (see the ESI†). Despite the less resolved data, all SAXS diagrams have a common pattern compatible with a similar self-assembly. Therefore, the



Scheme 2 Hydrolysis of arylboronate alkylglucoside.

herringbone packing constitutes a general feature involved in the self-assembling process of such molecules.

Water-sensitivity

In our preliminary study, we demonstrated that these organogels get disrupted upon contact with water.²⁴ At this time, we showed that this water-sensitivity originated from the hydrolysis of the boronate function (Scheme 2). Then, it leads back to the corresponding arylboronic acid and alkylglucoside. These two compounds are not gelators themselves; thus, it finally ends to a solution. Furthermore, within other contexts, arylboronate function hydrolysis has also been described.^{42,45}

Here, we investigated more thoroughly the water-sensitivity of these novel organogels with the aim to determine the molecular parameters modulating the gel disruption upon contact with water. This comparative study was performed using gels prepared with toluene, following two protocols: (A) addition of a small amount of water (5% v/v) on the top of the gels and visual follow-up until total disruption (over a maximum of one week); (B) video follow-up of a piece of gel (cylinder of $\varnothing 2.4 \times 1$ cm) immersed in a large excess of water. Then, image treatment permitted graphs describing the gel disruption against time to be plotted.

The addition of 5% v/v of water permitted to establish that the length of the alkyl chain dramatically impacts the duration of the water-induced disruption of the toluene-based gels (Protocol A, Table 4). Indeed, the gel obtained with the propyl derivative (**1a**) disappeared in 1h30 followed by the one from the butyl derivative **2a** (3h00). Under the same conditions, the corresponding gels from hexyl and octyl counterparts (**3a** and **4a**) were kept untouched even after one week of water exposure.

Table 4 Water-sensitivity in the presence of 5% v/v of water^a

| Compound | Time (h) |
|-----------|---------------------|
| 1a | 1 : 30 |
| 2a | 3 : 00 |
| 3a | > Week ^b |
| 4a | > Week ^b |
| 2b | 8 : 00 |
| 4b | > Week ^b |
| 2c | 4 : 00 |
| 4c | > Week ^b |

^a Gels were prepared using toluene at the MGC. ^b No hydrolysis after one week.

The substitution of the aromatic ring of boronate also modulated the water-sensitivity, increasing the disruption time from 3h00 (**2a**) to 8h00 (**2b**) and 4h00 (**2c**). The insertion of a bulky *o*-Me (**2b**) group induced a steric hindrance which contributes to a protective effect on the boronate function in the self-assembly. It is noteworthy that the steric hindrance brought by the extra *o*-Me (**2b**) group decreased much more the water sensitivity of these gels than the electron donating *p*-OMe group (**2c**). Nevertheless, increasing the alkyl chain to octyl (**4c** and **4b**) avoids the hydrolytic disruption under these conditions, indicating that the aglycone chain length has a major influence here.

The second protocol (B) allowed the behaviour of these gels to be evaluated in the presence of a large excess of water. A piece of gel was immersed in water and its disappearance was recorded using a camera placed aside of the gels (see the ESI† for GIF files). Therefore, the collected images were representative of the remaining gel and data treatment permitted graphs describing the disruption progress against time (% of remaining gel against time (min)) to be plotted. Fig. 7 reports the water-sensitivity of toluene-based organogels as a function of the chain length. For all experiments, we fixed the organogelator concentrations to 12 mg mL⁻¹ for the comparison purpose. Here, the water, surrounding the bottom and the sides of the gel discs, induced gel disappearance in few minutes to few hours. In addition, the process turned out to be isotropic, as the shape of the gels remained similar with time. For the previous study with 5% v/v of water, the propyl derivative (**1a**) was the fastest to break down (80% of gel in 20 minutes). The butyl derivative (**2a**) required more than double time (53 min) to lose 80% of the gel state. At this stage, one can imagine that longer chains would lead to lower water sensitivity. However, the octyl derivative (**4a**) appeared to disrupt faster than the hexyl counterpart (**3a**) (**4a**, 80% in 80 min; **3a**, 80% in 185 min).

Then, we compared organogelators bearing the same alkyl chain (*n*-butyl) but different substituents on the phenylboronate moiety (**2a**, **b**, and **c**) (Fig. 8). For the comparison purpose, the concentration was fixed to 16 mg mL⁻¹. Note that the gel obtained with **2c** (*p*-OMe) behaved differently than the two others at the beginning of the water-sensitivity experiments.

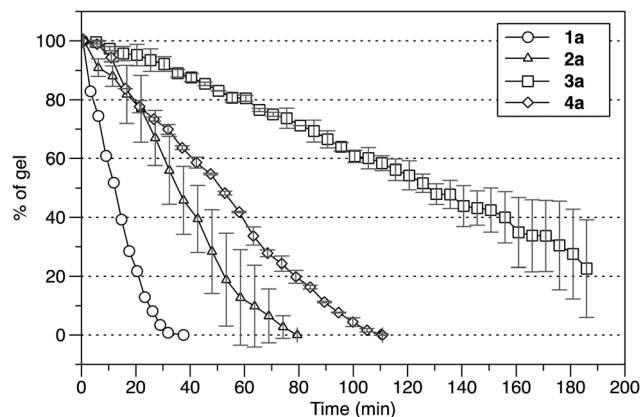


Fig. 7 Percentages of the remaining gel against time (min) after immersion in water. Gels prepared using **1a–4a** at 12 mg mL⁻¹ in toluene.

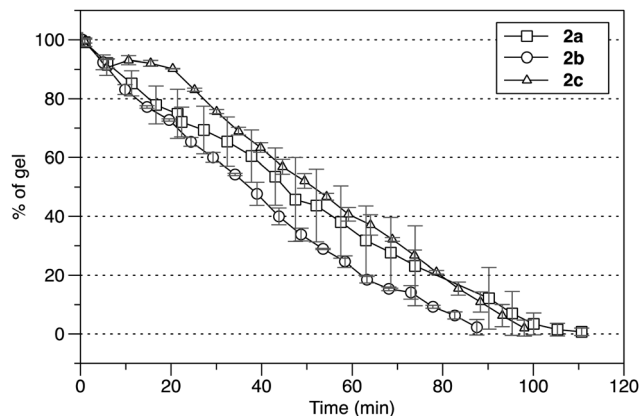


Fig. 8 Percentages of the remaining gel against time (min) after immersion in water. Gels prepared using **2a**, **2b**, and **2c** at 16 mg mL^{-1} in toluene.

For some of the gels, in particular with **2c**, determining the accurate boundaries of the gel disc is optically complex. For such gels, a halo of solvent appears to be captured below and in the vicinity of the gel; this leads to an overestimation of the actual size of the gel as the boundary which is optically detected includes this halo. As a consequence, even though the gel continuously disappears, an apparent flattening of the curve can be obtained (Fig. 8, **2c**). Regarding the time to reach 80% of disruption, surprisingly, the gel from **2b** showed the fastest disruption and those from **2a–2c** provided very similar results with disruption times longer by only 20 minutes.

To elucidate the main factors determining the water-sensitivity, we envisaged several plausible explanations: (1) the water-sensitivity would be related to the electrophilicity of the boronate function itself; (2) different modes of packing may conduce to different hydrolysis rates; (3) differences in the mechanical properties of the gels would be responsible for the water-sensitivity differences; (4) the fibre networks (size, density, *etc.*) would facilitate or not the water entry into the gels.

Shimida *et al.* already explained the stability of some arylboronates against water within an organic synthesis context, by comparing orbital energy levels.³⁹ Similarly, we established the energy levels of molecular orbitals for each compound **1a–4a** at the $\omega\text{B97XD/cc-pVTZ}$ level of theory (see the ESI,[†] Table S6.3 and Fig. S6.3). All compounds showed very close LUMO energies confirming that the different arylboronate functions should show similar reactivities that do not depend on the aglycone alkyl chain. The same conclusion has raised by considering the water-sensitivities of the gels from **2a**, **2b** and **2c**. Indeed, **2c** should provide the least water-sensitive organogel when examining the relative LUMO energy levels (see the ESI,[†] Table S6.3). However, gels with **2b** demonstrated a weaker water-sensitivity than those with **2a** and **2c** (protocol A), and these three gels (in toluene) reached close disruption times after immersion in water (protocol B). Therefore, these evolutions over time support influences of other factors than the electrophilicity of the boronate function. As showed here in earlier paragraphs, SAXS studies concluded in a very similar mode of packing for all organogelators. Thus, the different hydrolysis rates are not

linked to different types of self-assembly. Very different rheological properties were also highlighted between gels obtained in toluene with **3a** and **4a** for instance. Indeed, the gel prepared using **3a** had stronger moduli than the ones for **4a**. Such a gap between both G' and G'' values can be associated with differences in the dynamics of disruption which may find an origin in an easier diffusion of water molecules in the gels. However, this trend is far from being general, for example, gels obtained with **2a** which showed a higher water-sensitivity than those using **3a** has though stronger moduli. Then, the main structural feature governing the water-sensitivity is the chain length of aglycone. One can conclude that increasing the global hydrophobicity of the self-assembly reduces the water-sensitivity. In fact, hexyl and octyl derivatives have a stronger resistance upon water contact compared to propyl and butyl, whatever the structure of the aryl boronate. The specific inversion of this trend between hexyl (**3**) and octyl (**4**) is hard to explain. As the disruption dynamics probably start first on the outside of the fibres, an explanation can be based on the comparison of the size and the shape of the fibre networks. The SEM images of the corresponding xerogels displayed clear differences which can facilitate or not the hydrolysis step. The gel in toluene with **4a** is characterised by thinner fibres than the gel obtained with **3a** which reduces the penetration of water molecules for the latter. Note also that compounds **1a**, **2a** and **2c** which led to the most water-sensitive gels present dense fibre networks constituted of thin fibres.

Finally, the water-sensitivity of these systems would be related to both the hydrophobicity of the self-assembly and the specific surfaces available for the water molecules to access the hydrolysable boronate function.

Conclusions

The synthesis of twelve arylboronate alkylglucosides was achieved in a single chemical step with excellent yields. This covered structural variations both at the anomeric position and on the aromatic ring. This series of potential or effective organogelators allowed evaluation of the impact of these structural variations at different scales both on the gelation ability and on the behaviour of the corresponding gels. One first conclusion raising from this work established that the conformation of the boronate function clearly modifies the gelation ability of such compounds. Rather planar conformations are required to obtain the gelation of toluene, ethyl myristate and cyclohexane at low to very low minimal gelation concentrations. The interesting properties of these series of organogelators come from their capacity to disrupt upon contact with water. Even if the hydrolysis of the boronate function remains at the origin of the gel disruption, the main structural feature that matters is the length of the alkyl chain aglycone. In general, the shorter the alkyl chain the higher is the water-sensitivity. In addition, careful analysis of the set of physicochemical data (rheology, SEM, SAXS) allowed identifying the nature of the fibre network also as a determining parameter for the water-sensitivity of these gels (more than the mode of packing or the intrinsic reactivity of the boronate function).

Therefore, this study provided important insights into the main structural features controlling the behaviour of this family of organogelators for both the gelation of apolar organic solvents and their water-sensitivity. Additional structural modifications and gelation conditions would contribute in the future to reach a great control and a better modulation of both the gelation and water-sensitivity properties of such organogels.

Experimental

General information

^1H NMR spectra (300 MHz, 400 MHz), ^{13}C NMR (75 MHz, 101 MHz), ^{19}F (282 MHz) and ^{11}B (96 MHz) were recorded using Bruker AV 300 and AV 400 spectrometers. Chemical shifts are given in ppm and coupling constants J in Hz. Multiplicities are presented as follows: s = singlet, d = doublet, t = triplet, q = quartet, quint = quintuplet, hex = hexuplet, m = multiplet, br = broad. The carbon bearing the boron atom was not observed due to the multiplet structure: 1-1-1-1 quadruplet for ^{11}B -bearing ^{13}C (80%) and 1-1-1-1-1-1 septuplet for ^{10}B -bearing ^{13}C (20%) and to the quadrupolar relaxation mechanism of both B isotopes.⁴⁶ Attribution numbers are related to the sugar nomenclature numbering. High-resolution mass spectra (HRMS) were recorded, either using a Bruker MaXis 4G spectrometer, an Agilent 6510 spectrometer, or a Thermo Fisher Q-Exactive spectrometer (Centre Régional de Mesures Physiques de l'Ouest, Rennes) using positive ion Electron-Spray ionization techniques. Melting points were measured using a melting point apparatus Stuart SMP10 and are uncorrected. The specific rotation (in $\text{deg cm}^3 \text{g}^{-1}$) was measured using a PerkinElmer-341 polarimeter.

Gel formation

The gels were prepared by mixing the appropriate amount of gelators into the chosen organic solvent at various concentrations in capped tubes. The tubes were heated at 60 °C (cyclohexane), 80 °C (toluene) or 120 °C (fatty esters) for 1 h or until clear solutions were obtained. Clear solutions were then cooled down to room temperature to allow the formation of a gel. The MGC (minimal gelation concentration) was determined as the lowest concentration leading to a complete gelation of the solvent (The concentration was reduced by 1 mg mL^{-1} from 20 mg mL^{-1} to the MGC).

Rheology

The organogel samples were presented under a disc form (4 cm diameter and a few mm of thickness, depending on the organogelators). Rheological measurements were performed using an Anton-Paar MCR301 equipped with an upper plate of 75 mm in diameter. Amplitude-sweep experiments were performed, where the frequency (ω) was fixed to 1 Hz and the amplitude deformation (γ) was gradually increased from 0 to 50% of shearing. The storage modulus G' and the loss modulus G'' were obtained at 25 °C.

Complementary frequency-sweep experiments were also performed and showed that G' is always bigger than G'' over the whole range of frequencies (0.05 Hz to 10 Hz).

Scanning electron microscopy (SEM)

Metallisation by Au/Pd. The scanning electron microscopy (SEM) images of xerogels were evaluated using a JEOL IT 300 Scanning Electron Microscope. Samples were collected and deposited on a Teflon plot. Each sample was examined at a voltage of 5 or 10 kV. Images were analysed using the SMileView software.

Small angle X-ray scattering (SAXS)

The xerogel samples were prepared into capillaries. SAXS experiments were performed using X-ray patterns collected using a Pilatus 300k (Dectris, Grenoble, France), mounted on a micro-source X-ray generator GeniX 3D (Xenocs, Sassenage, France) operating at 30 watts. The monochromatics CuK_α radiation is of $\lambda = 1.541 \text{ \AA}$. The diffraction patterns were therefore recorded for reciprocal spacing $q = 4\pi \times \sin \theta/\lambda$ in a range of repetitive distances from 0.015 \AA^{-1} (418 \AA) to 1.77 \AA^{-1} (8 \AA). Images were transformed to graphics using the software program Fit2D (ESRF).

Hydrolysis experiments

Procedure A. 5% v/v of water was added on the top of gels formed in toluene (1 mL). Gelators were used at their minimal gelation concentrations. The disappearance of the gels was observed by eyes. Procedure B. Gels were prepared into 5 mL beakers, making possible to obtain gels approximately 10 mm in height and 24 mm in diameter. Gels were then unmoulded using a needle. Gels were immersed in water and maintained in place by a rod. A camera was installed to view the gel from the side and pictures were taken every 10 seconds. The images obtained were processed using the ImageJ software permitting the % of remaining gel to be plotted against time.

Computational details

Computational studies were carried out on the 12-core Apple computing cluster using density functional theory (DFT) methods, as instituted in the Gaussian 09 (version D.01) program, tightening self-consistent field convergence thresholds (10^{-8} a.u.).⁴⁷ The preliminary results from several hybrid functional/basis combinations have been compared (see the ESI,† Table S6.1). All arylboronate alkylglucosides were optimized at $\omega\text{B97XD/cc-pVTZ}$ and $\text{B3LYP/6-311+G(d,p)}$ levels of theory and the first $\omega\text{B97XD/cc-pVTZ}$ was selected to consider dispersion forces.^{48,49} So, torsion, distances, molecular orbital energies were given with this first combination as shown in Fig. 2 (see the ESI,† Table S6.2). The vibrational analysis was performed at the same levels of theory to confirm that the optimized geometry is a true minimum (no imaginary frequency). Then the evolution and convergence of geometric optimizations and energy minimization of the frontier molecular orbitals were visualized and analysed using GaussView v5.2 in particular for distances and dihedral angles (ESI,† Table S6.2 and Fig. S6.3).⁵⁰

General procedure for the synthesis of boronate glucosides

Procedure A. In a 25 mL round bottom flask, alkylglucoside (0.3 mmol) and boronic acid (0.3 mmol) were added. The mixture was then stirred in a Kugelrohr distillation apparatus

at 90 °C under 0.1 mbars for 15 min to obtain the pure product. Compounds were washed by diisopropylether when necessary.

Procedure B. In a 25 mL round bottom flask, alkylglucoside (0.3 mmol) and boronic acid (0.3 mmol) were added. Toluene (15 mL) was added, and the reaction mixture was heated under stirring at reflux in a Dean-Stark Apparatus. After 5 h, the toluene was evaporated at a reduced pressure to afford pure products. Compounds were washed by diisopropylether when necessary.

Compounds **2a**, **3a**, and **4a** were already described.²⁴

***n*-Propyl-β-D-glucopyranoside 4,6-phenylboronate 1a.** 89 mg (96%). White solid; m.p. = 184–188 °C. $[α]_D = -52$ (C 1, CH₂Cl₂). ¹H NMR (300 MHz, CDCl₃) δ 7.85–7.77 (m, 2H), 7.48–7.40 (m, 1H), 7.38–7.32 (m, 2H), 4.44 (d, *J* = 7.7 Hz, 1H, H1), 4.30 (dd, *J* = 10.4, 5.4 Hz, 1H, H6), 4.01 (t, *J* = 10.4 Hz, 1H, H6), 3.88 (dt, *J* = 9.5, 6.8 Hz, 1H, OCH₂), 3.81–3.71 (m, 2H, H3 H4), 3.62–3.48 (m, 3H, OCH₂ H2 H5), 2.81 (brs, 1H, OH), 2.53 (brs, 1H, OH), 1.68 (hex, *J* = 7.3 Hz, 2H), 0.96 (t, *J* = 7.4 Hz, 3H). ¹³C NMR (75 MHz, CDCl₃) δ 134.3, 131.4, 127.8, 103.4, 75.1 (C1), 74.7 (C3), 74.3 (C4), 72.3 (C5), 68.7 (OCH₂), 64.2 (C6), 23.0, 10.5. The carbon α to the boron atom was not observed. ¹¹B NMR (96 MHz, CDCl₃) δ 27.0. HRMS (ESI+) (M + Na)⁺ calcd for C₁₅H₂₁O₆¹¹BNa 331.1323, found 331.1324.

***n*-Butyl-β-D-glucopyranoside 4,6-*o*-methylphenylboronate 2b.** 98 mg (97%). White solid; m.p. = 157–159 °C. $[α]_D = -62$ (C 1, CH₂Cl₂). ¹H NMR (300 MHz, CDCl₃) δ 7.75 (d, *J* = 7.0 Hz, 1H), 7.30 (t, *J* = 7.2 Hz, 1H), 7.15 (t, *J* = 7.0 Hz, 1H), 7.14 (d, *J* = 7.3 Hz, 1H), 4.42 (d, *J* = 7.7 Hz, 1H, H1), 4.28 (dd, *J* = 10.4, 5.3 Hz, 1H, H6), 3.99 (t, *J* = 10.3 Hz, 1H, H6), 3.91 (dt, *J* = 10.0, 6.8 Hz, 1H, OCH₂), 3.83–3.67 (m, 2H, H4 H2), 3.65–3.44 (m, 3H, H3 OCH₂ H5), 3.22 (brs, 1H, OH), 3.06 (brs, 1H, OH), 2.51 (s, 3H, CH₃), 1.65 (quint, *J* = 7.2 Hz, 2H), 1.40 (hex, *J* = 7.4 Hz, 2H), 0.94 (t, *J* = 7.3 Hz, 3H). ¹³C NMR (75 MHz, CDCl₃) δ 143.9, 135.0, 130.3, 129.8, 124.5, 103.0 (C1), 74.7 (C4), 74.2 (C3), 73.8 (C2), 70.0 (OCH₂), 68.2 (C5), 63.7 (C6), 31.3, 22.3, 18.8, 13.5. The carbon α to the boron atom was not observed. ¹¹B NMR (96 MHz, CDCl₃) δ 28.2. HRMS (ESI+) (M + Na)⁺ calcd for C₁₇H₂₅O₆¹¹BNa 359.1636, found 359.1637.

***n*-Butyl-β-D-glucopyranoside 4,6-*p*-methoxyphenylboronate 2c.** 101 mg (96%). White solid; m.p. = 178–180 °C. $[α]_D = -69$ (C 1, CH₂Cl₂). ¹H NMR (300 MHz, CDCl₃) δ 7.75 (d, *J* = 8.6 Hz, 2H), 6.87 (d, *J* = 8.6 Hz, 2H), 4.41 (d, *J* = 7.7 Hz, 1H, H1), 4.26 (dd, *J* = 10.4, 5.4 Hz, 1H, H6), 4.00–3.86 (m, 2H, H6 OCH₂), 3.80 (s, 3H, OCH₃), 3.76–3.73 (m, 2H, H4 H3), 3.46–3.61 (m, 3H, OCH₂ H2 H5), 3.31 (brs, 1H, OH), 3.06 (brs, 1H, OH), 1.62 (quint, *J* = 7 Hz, 2H), 1.39 (hex, *J* = 7.3 Hz, 2H), 0.93 (t, *J* = 7.4 Hz, 3H). ¹³C NMR (75 MHz, CDCl₃) δ 161.8, 135.6, 122.2 (br), 112.9, 102.9 (C1), 74.7 (C4), 74.1 (C3), 73.8 (C2), 70.0 (OCH₂), 68.3 (C5), 63.7 (C6), 54.8, 31.3, 18.8, 13.5. The carbon α to the boron atom was not observed. ¹¹B NMR (96 MHz, CDCl₃) δ 27.7. HRMS (ESI+) (M + Na)⁺ calcd for C₁₇H₂₅O₇¹¹BNa 375.1585, found 375.1587.

***n*-Butyl-β-D-glucopyranoside 4,6-*o*-dimethylphenylboronate 2d.** 102 mg (97%). Colorless oil. $[α]_D = -62$ (C 1, CH₂Cl₂). ¹H NMR (300 MHz, CDCl₃) δ 7.12 (t, *J* = 7.5 Hz, 1H), 6.94 (d, *J* = 7.6 Hz, 2H), 4.42 (d, *J* = 7.8 Hz, 1H, H1), 4.28 (dd, *J* = 10.4, 5.3 Hz, 1H, H6), 4.01 (t, *J* = 10.4 Hz, 1H, H6), 3.89 (dd, *J* = 9.4, 6.9 Hz, 2H, H4_{OCH₂}), 3.78

(t, *J* = 9.2 Hz, 1H, H3), 3.73–3.44 (m, 3H, OCH₂ H2 H5), 3.20 (brs, 1H, OH), 2.95 (brs, 1H, OH), 2.34 (s, 6H, CH₃), 1.63 (quint, *J* = 7.2 Hz, 2H), 1.39 (hex, *J* = 7.0 Hz, 2H), 0.94 (t, *J* = 7.4 Hz, 3H). ¹³C NMR (75 MHz, CDCl₃) δ 140.4, 133.6 (br), 129.0, 126.5, 103.4 (C1), 75.0 (C4), 75.0 (C3), 74.0 (C2), 70.4 (OCH₂), 68.7 (C5), 64.4 (C6), 31.7, 22.3, 19.2, 13.9. The carbon α to the boron atom was not observed. ¹¹B NMR (96 MHz, CDCl₃) δ 31.2. HRMS (ESI+) (M + Na)⁺ calcd for C₁₈H₂₇O₆¹¹BNa 373.1792, found 373.1792.

***n*-Butyl-β-D-glucopyranoside 4,6-*o*-trifluoromethylphenylboronate 2e.** 114 mg (98%). Colorless oil. $[α]_D = -62$ (C 1, CH₂Cl₂). ¹H NMR (300 MHz, CDCl₃) δ 7.71–7.60 (m, 2H), 7.54–7.44 (m, 2H), 4.44 (d, *J* = 7.7 Hz, 1H, H1), 4.29 (dd, *J* = 10.4, 5.3 Hz, 1H, H6), 4.01 (t, *J* = 10.4 Hz, 1H, H6), 3.90 (dt, *J* = 9.5, 6.8 Hz, 1H, OCH₂), 3.80 (t, *J* = 9.2 Hz, 1H, H4), 3.70 (t, *J* = 9.0 Hz, 1H, H3), 3.63–3.48 (m, 3H, OCH₂ H2 H5), 3.06 (brs, 1H, OH), 2.88 (brs, 1H, OH), 1.63 (quint, *J* = 6.9 Hz, 2H), 1.40 (hex, *J* = 7.2 Hz, 2H), 0.93 (t, *J* = 7.3 Hz, 3H). ¹³C NMR (75 MHz, CDCl₃) δ 134.4, 133.85 (q, *J* = 31.2 Hz), 131.3, 130.25, 126.0 (q, *J* = 5.0 Hz), 125.2 (q, *J* = 273.4 Hz), 103.9 (C1), 75.6 (C4), 75.3 (C3), 74.5 (C2), 70.9 (OCH₂), 68.8 (C5), 65.0 (C6), 32.2, 19.7, 14.35. The carbon α to the boron atom was not observed. ¹⁹F NMR (282 MHz, CDCl₃) δ -59.4. ¹¹B NMR (96 MHz, CDCl₃) δ 28.7. HRMS (ESI+) (M + Na)⁺ calcd for C₁₇H₂₂¹¹BF₃O₆Na 413.1353, found 413.1358.

***n*-Octyl-β-D-glucopyranoside 4,6-*o*-methylphenylboronate 4b.** 112 mg (95%). White solid; m.p. = 142–144 °C. $[α]_D = -70$ (C 1, CH₂Cl₂). ¹H NMR (300 MHz, CDCl₃) δ 7.75 (dd, *J* = 7.6, 1.6 Hz, 1H), 7.30 (t, *J* = 7.1 Hz, 1H), 7.16 (t, *J* = 6.9 Hz, 1H), 7.14 (d, *J* = 7.4 Hz, 1H), 4.44 (d, *J* = 7.7 Hz, 1H, H1), 4.31 (dd, *J* = 10.4, 5.4 Hz, 1H, H6), 4.01 (t, *J* = 10.4 Hz, 1H, H6), 3.91 (dt, *J* = 9.3, 6.8 Hz, 1H, OCH₂), 3.84–3.68 (m, 2H, H3 H4), 3.63–3.50 (m, 3H, OCH₂ H2 H5), 2.75 (brs, 1H, OH), 2.53 (brs, 1H, OH), 2.51 (s, 3H, CH₃), 1.64 (quint, *J* = 7.0 Hz, 2H), 1.20–1.43 (m, 10H), 0.88 (t, *J* = 6.7 Hz, 3H). ¹³C NMR (75 MHz, CDCl₃) δ 144.9, 135.9, 131.3, 130.8, 125.4, 103.8 (C1), 75.6 (C4), 75.2 (C3), 74.7 (C2), 71.3 (OCH₂), 69.1 (C5), 64.6 (C6), 32.4, 30.2, 29.9, 29.8, 26.5, 23.2, 23.1, 14.7. The carbon α to the boron atom was not observed. ¹¹B NMR (96 MHz, CDCl₃) δ 27.8. HRMS (ESI+) (M + Na)⁺ calcd for C₂₁H₃₃O₆¹¹BNa 415.2262, found 415.2263.

***n*-Octyl-β-D-glucopyranoside 4,6-*p*-methoxyphenylboronate 4c.** 120 mg (98%). White solid; m.p. = 156–158 °C. $[α]_D = -51$ (C 1, CH₂Cl₂). ¹H NMR (300 MHz, CDCl₃) δ 7.75 (d, *J* = 8.5 Hz, 2H), 6.87 (d, *J* = 9.0 Hz, 2H), 4.42 (d, *J* = 7.7 Hz, 1H, H1), 4.26 (dd, *J* = 10.4, 5.3 Hz, 1H, H6), 3.97 (t, *J* = 10.2 Hz, 1H, H6), 3.88 (dd, *J* = 9.4, 6.9 Hz, 1H, OCH₂), 3.81 (s, 3H, OCH₃), 3.77–3.73 (m, 2H, H3 H4), 3.46–3.62 (m, 3H, H2 OCH₂ H5), 3.18 (brs, 1H, OH), 2.93 (brs, 1H, OH), 1.63 (quint, *J* = 7.0 Hz, 2H), 1.20–1.40 (m, 10H), 0.88 (t, *J* = 6.2 Hz, 3H). ¹³C NMR (75 MHz, CDCl₃) δ 162.2, 136.1, 113.4, 103.4 (C1), 75.1 (C4), 74.6 (C3), 74.3 (C2), 70.8 (OCH₂), 68.7 (C5), 64.1 (C6), 55.2, 31.9, 29.7, 29.5, 29.3, 26.0, 22.8, 14.2. The carbon α to the boron atom was not observed. ¹¹B NMR (96 MHz, CDCl₃) δ 21.4. HRMS (ESI+) (M + Na)⁺ calcd for C₂₁H₃₃O₇¹¹BNa 431.2212, found 431.2213.

***n*-Octyl-β-D-glucopyranoside 4,6-*o*-dimethylphenylboronate 4d.** 118 mg (97%). Colorless oil. $[α]_D = -53$ (C 1, CH₂Cl₂). ¹H NMR (300 MHz, CDCl₃) δ 7.12 (t, *J* = 7.5 Hz, 1H), 6.95 (d, *J* = 7.6 Hz, 2H), 4.46 (d, *J* = 7.7 Hz, 1H, H1), 4.31 (dd, *J* = 10.5,

5.4 Hz, 1H, H6), 4.04 (t, $J = 10.4$ Hz, 1H, H6), 3.91 (dt, $J = 9.5, 6.2$ Hz, 1H, OCH₂), 3.81 (t, $J = 9.2$ Hz, 1H, H4), 3.71 (td, $J = 9.2, 2.1$ Hz, 1H, H3), 3.66–3.49 (m, 3H, H5 H2 OCH₂), 2.82 (d, $J = 2.2$ Hz, 1H, OH), 2.56 (d, $J = 2.4$ Hz, 1H, OH), 2.35 (s, 6H, CH₃), 1.64 (quint, $J = 7.1$ Hz, 2H), 1.29 (m, 10H), 0.89 (t, $J = 6.5$ Hz, 3H). ¹³C NMR (101 MHz, CDCl₃) δ 140.4, 133.6 (br), 129.0, 126.5, 103.4 (C1), 75.0 (C4), 75.0 (C3), 74.0 (C2), 70.8 (OCH₂), 68.7 (C5), 64.4 (C6), 31.0, 29.7, 29.5, 29.3, 26.0, 22.8, 22.3, 14.2. The carbon α to the boron atom was not observed. ¹¹B NMR (96 MHz, CDCl₃) δ 31.15. HRMS (ESI+) (M + Na)⁺ calcd for C₂₂H₃₅O₆¹¹BNa 429.2418, found 429.2421.

***n*-Octyl- β -D-glucopyranoside 4,6-*o*-trifluoromethylphenylboronate 4e.** 130 mg (97%). Colorless oil. $[\alpha]_D = -55$ (C 1, CH₂Cl₂). ¹H NMR (300 MHz, CDCl₃) δ 7.80 (d, $J = 8.1$ Hz, 2H), 7.59 (t, $J = 7.9$ Hz, 2H), 4.45 (d, $J = 7.6$ Hz, 1H, H1), 4.29 (dd, $J = 10.3, 5.4$ Hz, 1H, H6), 4.01 (t, $J = 10.3$ Hz, 1H, H6), 3.89 (dt, $J = 9.5, 6.9$ Hz, 1H, OCH₂), 3.80 (t, $J = 9.2$ Hz, 1H, H4), 3.71 (t, $J = 9.2$ Hz, 1H, H3), 3.62–3.50 (m, 3H, OCH₂ H2 H5), 1.63 (quint, $J = 7.0$ Hz, 2H), 1.29 (m, 10H), 0.89 (t, $J = 6.9$ Hz, 3H). ¹³C NMR (75 MHz, CDCl₃) δ 134.0, 133.4 (q, $J = 30.9$ Hz), 130.9, 129.85, 125.6 (q, $J = 5.1$ Hz), 124.76 (q, $J = 273.4$ Hz), 103.5 (C1), 75.2 (C4), 74.9 (C3), 74.1 (C2), 70.85 (OCH₂), 68.4 (C5), 64.6 (C5), 31.9 (C6), 29.7, 29.5, 29.3, 26.0, 22.8, 14.2. The carbon α to the boron atom was not observed. ¹⁹F NMR (282 MHz, CDCl₃) δ -59.4. ¹¹B NMR (96 MHz, CDCl₃) δ 28.3. HRMS (ESI+) (M + Na)⁺ calcd for C₂₁H₃₀¹¹BF₃O₆Na 469.1979, found 469.1982.

Author contributions

A. D. L. and N. O.-M. carried out the experiments with supervisory guidance from F. B., A. S.-J. and L. L. A. S.-J. proposed and supervised the rheometric experiments. F. A. carried out and analyzed the SAXS measurements with input from L. L. J.-P. G. performed the VT-NMR experiments with L. L. O. T. implemented the computational studies with input from L. L. L. L. and F. B. conceptualized and supervised the study, and wrote the original draft. All authors contributed to the final manuscript.

Conflicts of interest

There are no conflicts to declare.

Acknowledgements

We acknowledge the Ministère de l'Éducation Nationale, de la Recherche et de la Technologie. The authors thank F. Gouttefangeas and L. Joanny from the CMEBA (Centre de Microscopie Electronique à Balayage et microAnalyse, Rennes) for assistance in recording SEM images.

Notes and references

- 1 L. Zeng, X. Lin, P. Li, F.-Q. Liu, H. Guo and W.-H. Li, *Prog. Org. Coat.*, 2021, **159**, 106417.
- 2 M. George and R. G. Weiss, *Acc. Chem. Res.*, 2006, **39**, 489–497.

- 3 D. J. Abdallah and R. G. Weiss, *Adv. Mater.*, 2000, **12**, 1237–1247.
- 4 P. R. A. Chivers and D. K. Smith, *Nat. Rev. Mater.*, 2019, **4**, 463–478.
- 5 E. R. Draper and D. J. Adams, *Chem*, 2017, **3**, 390–410.
- 6 S. S. Babu, V. K. Praveen and A. Ajayaghosh, *Chem. Rev.*, 2014, **114**, 1973–2129.
- 7 D. Rosa Nunes, M. Raynal, B. Isare, P.-A. Albouy and L. Bouteiller, *Soft Matter*, 2018, **14**, 4805–4809.
- 8 D. Rosa Nunes, M. Reche-Tamayo, E. Ressouche, M. Raynal, B. Isare, P. Foury-Leylelian, P.-A. Albouy, P. Brocorens, R. Lazzaroni and L. Bouteiller, *Langmuir*, 2019, **35**, 7970–7977.
- 9 M. Raynal and L. Bouteiller, *Chem. Commun.*, 2011, **47**, 8271–8273.
- 10 Y. Lan, M. G. Corradini, R. G. Weiss, S. R. Raghavan and M. A. Rogers, *Chem. Soc. Rev.*, 2015, **44**, 6035–6058.
- 11 J. Morris, J. Bietsch, K. Bashaw and G. Wang, *Gels*, 2021, **7**, 24.
- 12 A. D. Ludwig, F. Berrée and L. Lemiègre, *Carbohydrate Chemistry*, The Royal Society of Chemistry, 2022, vol. 45, pp. 379–415.
- 13 A. Prathap and K. M. Sureshan, *Langmuir*, 2019, **35**, 6005–6014.
- 14 T. Ishi-i and S. Shinkai, *Top. Curr. Chem.*, 2005, **258**, 119–160.
- 15 Y. Kubo, W. Yoshizumi and T. Minami, *Chem. Lett.*, 2008, **37**, 1238–1239.
- 16 F. Xu, L. Pfeifer, S. Crespi, F. K.-C. Leung, M. C. A. Stuart, S. J. Wezenberg and B. L. Feringa, *J. Am. Chem. Soc.*, 2021, **143**, 5990–5997.
- 17 E. Suarez-Picado, M. Coste, J.-Y. Runser, M. Fosseppe, A. Carvalho, M. Surin, L. Jierry and S. Ulrich, *Biomacromolecules*, 2022, **23**, 431–442.
- 18 S. J. Ren, H. Q. Liang, P. P. Sun, Y. N. Gao and L. Q. Zheng, *New J. Chem.*, 2020, **44**, 1609–1614.
- 19 A. Nuthanakanti, *New J. Chem.*, 2019, **43**, 13447–13456.
- 20 A. Nuthanakanti and S. G. Srivatsan, *ACS Appl. Mater. Interfaces*, 2017, **9**, 22864–22874.
- 21 J. A. Foster, R. M. Edkins, G. J. Cameron, N. Colgin, K. Fucke, S. Ridgeway, A. G. Crawford, T. B. Marder, A. Beeby, S. L. Cobb and J. W. Steed, *Chem. – Eur. J.*, 2014, **20**, 279–291.
- 22 C. D. Jones and J. W. Steed, *Chem. Soc. Rev.*, 2016, **45**, 6546–6596.
- 23 E. R. Draper and D. J. Adams, *Chem. Commun.*, 2016, **52**, 8196–8206.
- 24 A. D. Ludwig, A. Saint-Jalmes, C. Mériadec, F. Artzner, O. Tasseau, F. Berrée and L. Lemiègre, *Chem. – Eur. J.*, 2020, **26**, 13927–13934.
- 25 A. M. Vibhute, V. Muvvala and K. M. Sureshan, *Angew. Chem., Int. Ed.*, 2016, **55**, 7782–7785.
- 26 F. Ono, O. Hirata, K. Ichimaru, K. Saruhashi, H. Watanabe and S. Shinkai, *Eur. J. Org. Chem.*, 2015, 6439–6447.
- 27 J. Morris, P. Kozlowski and G. Wang, *Langmuir*, 2019, **35**, 14639–14650.
- 28 A. Chen, L. P. Samankumara, C. Garcia, K. Bashaw and G. Wang, *New J. Chem.*, 2019, **43**, 7950–7961.
- 29 A. Chen, I. S. Okafor, C. Garcia and G. Wang, *Carbohydr. Res.*, 2018, **461**, 60–75.

- 30 G. Wang, A. Chen, H. P. R. Mangunuru and J. R. Yerabolu, *RSC Adv.*, 2017, **7**, 40887–40895.
- 31 J. Kowalczyk, M. Bielejewski, A. Lapinski, R. Luboradzki and J. Tritt-Goc, *J. Phys. Chem. B*, 2014, **118**, 4005–4015.
- 32 H. Xu, J. Song, T. Tian and R. Feng, *Soft Matter*, 2012, **8**, 3478–3486.
- 33 J. Tritt-Goc and J. Kowalczyk, *Langmuir*, 2012, **28**, 14039–14044.
- 34 K. Sakurai, Y. Jeong, K. Koumoto, A. Friggeri, O. Gronwald, S. Sakurai, S. Okamoto, K. Inoue and S. Shinkai, *Langmuir*, 2003, **19**, 8211–8217.
- 35 O. Gronwald and S. Shinkai, *Chem. – Eur. J.*, 2001, **7**, 4329–4334.
- 36 N. Kameta, M. Masuda and T. Shimizu, *Chem. Commun.*, 2015, **51**, 11104–11107.
- 37 N. Kameta, K. Ishikawa, M. Masuda, M. Asakawa and T. Shimizu, *Chem. Mater.*, 2012, **24**, 209–214.
- 38 N. Shimada, K. Fukuhara, S. Urata and K. Makino, *Org. Biomol. Chem.*, 2019, **17**, 7325–7329.
- 39 N. Shimada, S. Urata, K. Fukuhara, T. Tsuneda and K. Makino, *Org. Lett.*, 2018, **20**, 6064–6068.
- 40 R. S. Mancini, J. B. Lee and M. S. Taylor, *J. Org. Chem.*, 2017, **82**, 8777–8791.
- 41 S. Uzan, D. Barış, M. Çolak, H. Aydın and H. Hoşgören, *Tetrahedron*, 2016, **72**, 7517–7525.
- 42 H. Li, H. Li, Q. Dai, H. Li and J.-L. Brédas, *Adv. Theory Simul.*, 2018, **1**, 1700015.
- 43 J.-D. Chai and M. Head-Gordon, *Phys. Chem. Chem. Phys.*, 2008, **10**, 6615–6620.
- 44 D. Heß and P. Klüfers, *Carbohydr. Res.*, 2011, **346**, 1752–1759.
- 45 M. Tanaka, A. Nakagawa, N. Nishi, K. Iijima, R. Sawa, D. Takahashi and K. Toshima, *J. Am. Chem. Soc.*, 2018, **140**, 3644–3651.
- 46 B. Wrackmeyer, *Prog. Nucl. Magn. Reson. Spectrosc.*, 1979, **12**, 227–259.
- 47 M. J. Frisch, G. W. Trucks, H. B. Schlegel, G. E. Scuseria, M. A. Robb, J. R. Cheeseman, G. Scalmani, V. Barone, G. A. Petersson, H. Nakatsuji, X. Li, M. Caricato, A. Marenich, J. Bloino, B. G. Janesko, R. Gomperts, B. Mennucci, H. P. Hratchian, J. V. Ortiz, A. F. Izmaylov, J. L. Sonnenberg, D. Williams-Young, F. Ding, F. Lipparini, F. Egidi, J. Goings, B. Peng, A. Petrone, T. Henderson, D. Ranasinghe, V. G. Zakrzewski, J. Gao, N. Rega, G. Zheng, W. Liang, M. Hada, M. Ehara, K. Toyota, R. Fukuda, J. Hasegawa, M. Ishida, T. Nakajima, Y. Honda, O. Kitao, H. Nakai, T. Vreven, K. Throssell, J. J. A. Montgomery, J. E. Peralta, F. Ogliaro, M. Bearpark, J. J. Heyd, E. Brothers, K. N. Kudin, V. N. Staroverov, T. Keith, R. Kobayashi, J. Normand, K. Raghavachari, A. Rendell, J. C. Burant, S. S. Iyengar, J. Tomasi, M. Cossi, J. M. Millam, M. Klene, C. Adamo, R. Cammi, J. W. Ochterski, R. L. Martin, K. Morokuma, O. Farkas, J. B. Foresman and D. J. Fox, Gaussian, Inc., Wallingford CT, 2016.
- 48 K. J. Donald, U. R. Gaillard and N. Walker, *J. Phys. Chem. A*, 2022, **126**, 5173–5185.
- 49 A. D. Becke, *J. Chem. Phys.*, 1993, **98**, 5648–5652.
- 50 R. Dennington, T. A. Keith and J. M. Millam, *GaussView, Version 5.2*, Semichem Inc., Shawnee Mission, KS, 2016.